MRS Communications (2018), 1 of 7
© Materials Research Society, 2018
doi:10.1557/mrc.2018.167

MRS Communications

Research Letter

Atomic-level insights through spectroscopic and transport measurements into the large-area synthesis of MoS_2 thin films

Hassana Samassekou, Asma Alkabsh, Kenneth Stiwinter, Avinash Khatri, and **Dipanjan Mazumdar,** Department of Physics, Southern Illinois University, Carbondale, IL 62901, USA

Address all correspondence to Dipanjan Mazumdar at **dmazumdar@siu.edu**

(Received 25 May 2018; accepted 6 August 2018)

Abstract

Several structure–property relationships are reported in large-area MoS_2 thin films to understand the effect of sulfur vacancies along with complementary first-principles calculations. X-ray diffraction and reflectivity measurements demonstrated that sputtered MoS_2 followed by a high-temperature sulfurization produced sharp film–substrate interface along with high crystalline order. Spectroscopic and transport measurements showed that removal of sulfur vacancies promoted A–B excitons, strong in-plane Raman modes, a sharp increase in dc resistivity, and strong photo-conducting behavior. We have clearly demonstrated that a hybrid method using magnetron sputtering can provide high-quality few-layer transition metal dichalcogenide films.

Introduction

MoS_2 remains one of the most extensively studied two-dimensional materials in the transition-metal-dichalcogenide (TMDC) family.[1] Structurally, these novel materials are stacked together by Van-der-Waals forces.[2] Among the many remarkable properties shown by TMDCs, the existence of a tunable band gap, from indirect (1.3 eV, bulk) to direct (1.8 eV, monolayer) for MoS_2[3], is one of the attractive property.[4] Therefore, many electronic[1] and optoelectronic applications[5] are envisioned for such materials. Several growth techniques, classified as either top-down or bottom-up approaches, have been elaborated for 2D materials fabrication. However, the existing challenge of synthesis of scalable and high-quality TMDCs such as MoS_2 persists.

Popularized by the discovery of graphene,[6] top-down techniques which include liquid phase exfoliation[7] and micromechanical exfoliation,[8] produce flakes of typical small lateral size (<10 µm).[9] Several large-area fabrication techniques have been elaborated to pave the way for the fabrication of scalable and controllable 2D materials. These methods consist of powder vaporization[10–13] of elements and compounds such as Mo, W, MoO_3, and $MoCl_5$, metal-organic chemical vapor deposition,[14] atomic layer deposition,[15] thermolysis,[16] and physical vaporization techniques such as pulse laser deposition,[17] molecular beam epitaxy,[18] and magnetron sputtering.[19] A common feature of all these methods involved high-temperature growth process, preferably in a sulfur-rich environment. A literature review on large-area growth approach of TMDCs is summarized in Table S.1.

Previously, we developed a growth strategy using a magnetron sputtering technique to produce large-area few-layer MoS_2 films.[20] We showed that a room temperature growth using a stoichiometric target followed by an annealing at close to 450–500 °C led to well-defined Raman peaks, along with sharp interface with the substrate. While simple, careful investigations also revealed the presence of substantial chemical and structural disorder in our films.[20,21] Compared with the spectroscopic features of single crystal and chemical vapor deposition grown MoS_2,[11] well-defined exciton peaks were missing in optical absorption along with broad and weak E^1_{2g} Raman peaks. Since sulfur has a strong role in promoting such features, we hypothesized that the sputtered films suffer from inhomogeneous sulfur distribution and vacancies. This motivated the current study of fabricating and investigating the properties of MoS_2 thin films in a sulfur-rich environment.

In this work, we report the evolution of the spectroscopic and transport properties of sputtered MoS_2 annealed in a sulfur-rich environment at various temperatures. We show that the sulfurization process generates sharp exciton peaks, strong Raman modes, promotes semiconducting behavior (transport and optical), and better photo-conducting behavior. Some of the experimental results were directly correlated to electronic structure calculations. Broadly speaking, our work provides clear evidence that a novel hybrid PVD-CVD process leads to high-quality MoS_2 thin films.

Experimental and theoretical methods

The sulfurization process was conducted via an ex-situ process involving a CVD-type process as shown in Fig. S.1. MoS_2 films were deposited on quartz and sapphire substrates using a high vacuum magnetron sputtering system (base pressure

Downloaded from https://www.cambridge.org/core. Karolinska Institutet University Library, on 17 Aug 2018 at 17:55:22, subject to the Cambridge Core terms of use, available at https://www.cambridge.org/core/terms. https://doi.org/10.1557/mrc.2018.167

1×10^{-9} Torr). Transparent quartz was chosen over Si/SiO_2 to enable optical absorption and large-area transport measurements. The first method (referred as M_1) refers to our earlier studies which consisted of sputtering a commercially available stoichiometric MoS_2 target at a rate of 7 secs/layer, followed by a post-deposition annealing treatment at 485 °C under high vacuum conditions.[20,21] M_2 method consisted of sputtering MoS_2 at a rate of 25 secs/layer followed by a post-deposition annealing treatment at various temperatures under sulfur and argon environment. Most of the samples were fabricated using this method and it is the focus of this work. The third method, M_3, examined a high-temperature sulfurization (850 °C) of room temperature sputtered Mo thin film. This method has been explored in the literature and employed here for comparison (see Table S.1).

The stoichiometry of the films was verified by electron energy dispersive spectroscopy (EDS). X-ray diffraction (XRD) and X-ray reflectivity (XRR) patterns were assessed using a high-resolution Rigaku Smart Lab X-ray diffractometer equipped with a channel-cut Ge (220) crystal to obtain a highly monochromatic Cu $K_{\alpha 1}$ radiation (see Supplementary material for additional details). Film thickness was inferred using XRR and Ellipsometry measurements. The absorption spectra were obtained using a Shimadzu UV3600 broadband optical spectrometer in the 190–1500 nm range. Raman measurements were performed with Nanophoton Raman-11 spectrometer using a 532 nm laser. Electronic transport and photo-conducting measurements were obtained by means of a LabVIEW program and a 2400 Keithley source. First-principles calculations[22] were performed using the augmented plane wave + local orbitals (APW + lo) method as implemented in the WIEN2k package[23] using the generalized gradient approximation (GGA) by Perdew–Burke–Ernzerhof.[24] Van-der-Waals interactions[25] were incorporated. Kramers–Kronig consistent optical properties were also computed using the WIEN2k package.

Results and discussion

The XRD data in Fig. 1 demonstrates the effect of different growth conditions on 12 nm thick MoS_2 films. The three different synthesis methods mentioned earlier (M_1, M_2, and M_3) are compared in Fig. 1(a). M_1 referred to the vacuum annealed process while M_2 and M_3 referred to the sulfurized MoS_2 and Mo process, respectively. Both sulfurized conditions (sample type M_2 and M_3 annealed at 850 °C) reveal only (000l) peaks up to (0008) which was suggestive of a strong crystalline, oriented growth whereas unsulfurized M_1 samples showed only a weak (0002) peak. The extracted XRD features (peak position, intensity, and full-width-at-half-maximum (FWHM)) and lattice parameters are tabulated in Table I. The interplanar spacing, which corresponds to half the lattice parameter, was extracted for all (000l) MoS_2 reflections. For reference, the data were compared with a simulated MoS_2 bulk structure with relative intensities presented for several (000l) reflections. The 2θ peak position of the (0002) MoS_2 reflection was very close to the bulk value (14.4°) for the sulfurized samples, indicative of better crystallization with the sulfurization process. Unsulfurized samples showed a lower 2θ value implying a larger out-of-plane lattice parameter, which was reported in our prior work.[20] The (0002) peak showed a dramatic increase in intensity by nearly a factor of 100 after high-temperature sulfurization. The increase in intensity is concomitant with a narrow FWHM as shown in Table I.

The XRR measurements for the sulfurized MoS_2 (M_2 type) was compared with vacuum annealed MoS_2 (M_1) in Fig. 1(b). The oscillatory pattern revealed that sharp substrate–film interface was achieved in sulfurized MoS_2.[20] A fit to the XRR curve can provide layer-specific information such as thickness, surface and interfacial roughness, and density. The extracted thickness and rms roughness values are shown in Fig. 1(b). More detailed information is provided in Fig. S2. Quantitatively, the sulfurized MoS_2 film showed similar surface roughness (~0.6 nm) as vacuum-annealed MoS_2 which is

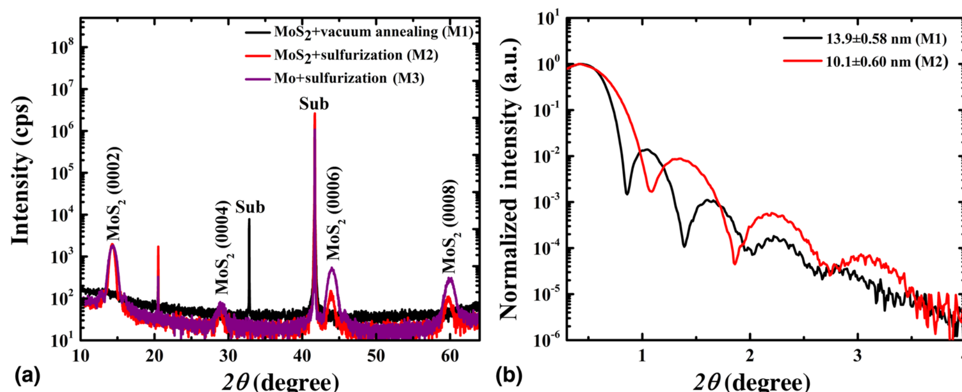

Figure 1. (a) XRD pattern of many-layer 12 nm-MoS_2 thin films grown on sapphire under different conditions. (b) XRR measurements for the sulfurized MoS_2 (M_2 type) compared with vacuum annealed MoS_2 (M_1).

Downloaded from https://www.cambridge.org/core. Karolinska Institutet University Library, on 17 Aug 2018 at 17:55:22, subject to the Cambridge Core terms of use, available at https://www.cambridge.org/core/terms. https://doi.org/10.1557/mrc.2018.167

Table I. MoS_2 2θ peak position as a function of growth conditions.

Parameters	M_1	M_2	M_3	Simulated bulk MoS_2
(*hkil*) indices		(0002)		
2θ position (deg)	13.52	14.28	14.34	14.39
Intensity (cps)	23	1956	1786	100
FWHM (deg)	2.1	0.65	0.93	–
Interplanar spacing (nm)	0.653	0.620	0.617	0.615
(*hkil*) indices		(0004)		
2θ position (deg)	–	28.93	29.10	29.01
Intensity (cps)	–	30	40	1.6
FWHM (deg)	–	0.73	1.04	–
Interplanar spacing (nm)	–	0.618	0.613	0.615
(*hkil*) indices		(0006)		
2θ position (deg)	–	44.00	43.96	44.14
Intensity (cps)	–	103	472	7.0
FWHM (deg)	–	0.81	1.04	–
Interplanar spacing (nm)	–	0.617	0.617	0.615
(*hkil*) indices		(0008)		
2θ position (deg)	–	59.76	60.08	60.13
Intensity (cps)	–	66	252	5.8
FWHM (deg)	–	0.87	1.18	–
Interplanar spacing (nm)	–	0.618	0.615	0.615

extremely encouraging. Therefore, we concluded that the sulfurization process did not degrade the sharp interfacial and surface properties of sputtered MoS_2 films while promoting high bulk properties. Similarly, large atomic force microscopy scans of sulfurized MoS_2 thin films demonstrated uniform low-roughness films with rms values of less than 1 nm, consistent with XRR analysis. Similar morphology was observed in 3–4 layer MoS_2 with a peak to valley height of nearly 2 nm which demonstrated that sulfurization of sputtered MoS_2 films can be used to grow high-quality few-layer MoS_2 (see Fig S.4 for details). Scanning electron microscopy (SEM) scans across different growth techniques revealed uniform films as shown in Fig. S.3 except for small sulfur particulates at the surface of sulfurized samples (M_2 and M_3), which were confirmed by electron EDS. The stoichiometry of the films for the three different growth conditions was summarized in Table S.2. AFM scans of sulfurized samples also demonstrated features consistent with sulfur patches observed in SEM measurements.

The effect of sulfurization temperature on the XRD pattern of many-layer (12 nm) MoS_2 deposited on fused quartz is shown in Fig. 2(a) and 2(b). The as-deposited films were sulfurized for 1 hr under sulfur and argon environment at temperatures ranging from 250 to 1000 °C. XRD data of four representative temperatures are shown. We observe that the (0002) peak, which is the strongest MoS_2 diffraction peak, was very weak or not observed for sulfurization temperatures below 650 °C. This was suggestive that low temperatures were not effective, whereas sulfurization at 850 and 1000 °C resulted in the appearance of higher (000*l*) MoS_2 peaks with low FWHM, indicative of strong crystalline structure at higher temperatures. Figure 2(b) illustrated the variation of (0002) peak position as a function of sulfurization temperature with detailed quantitative analysis shown in Table S.3. The peak position of the (0002) MoS_2 reflection progressively reached the bulk value ($c = 12.3$ Å) at 850 °C while the sample at 1000 °C appears to have lower (but close) than bulk lattice parameter. While it was inconclusive from this data alone, it indicated that very high sulfurization temperatures (above 850 °C from this study) might be detrimental to the MoS_2 structure and consistent with some other characterizations shown in later discussions. The structural characteristics of samples

Downloaded from https://www.cambridge.org/core. Karolinska Institutet University Library, on 17 Aug 2018 at 17:55:22, subject to the Cambridge Core terms of use, available at https://www.cambridge.org/core/terms. https://doi.org/10.1557/mrc.2018.167

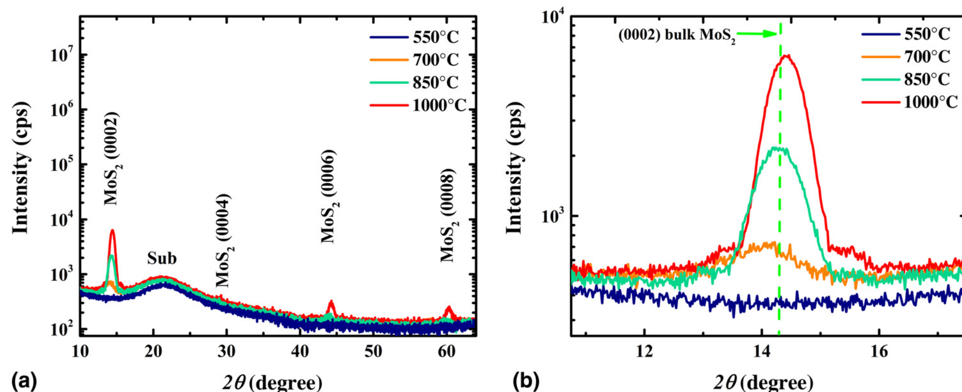

Figure 2. (a) XRD pattern of many-layer sputter deposited MoS_2 on fused quartz sulfurized at different temperatures as indicated. (b) Variation in many-layer MoS_2 (0002) peak position as a function of sulfurization temperature.

grown on different substrates (Si/SiO_2, quartz, and sapphire) are compared in Table S.4.

In Fig. 3(a) we show the absorption spectra of several 12 nm MoS_2 thin films as a function of sulfurization temperature. The most noteworthy change was the appearance of strong A, B (both around 2 eV as indicated) and C (around 2.7 eV) excitons as the temperature increased. A substantial change of excitonic energy position, intensity, and linewidth was also observed with increasing sulfurization temperature. These excitons correspond to the direct transition at K point in the Brillouin zone, from the split-valence band maximum (due to the spin-orbital splitting) to the conduction band minimum.[26] In-plane orbitals, such as S p_x and p_y, Mo d_{xy}, and d_{x^2}—x^2, which are responsible for valence band states at K point[27] are more sensitive to defects in the form of sulfur vacancies. The absence of sharp excitons in vacuum-annealed MoS_2 thin films is another strong evidence of sulfur vacancies in the films. The evolution of MoS_2 A–B excitons as a function of sulfurization temperature is shown in the inset figure (raw data shown in Table S.5). A clear red-shift of excitonic energy position at higher growth temperatures is noted which is consistent with the lattice relaxation observed in XRD measurements. Even though we did not directly measure the in-plane lattice constant, the data hint that the relaxation of lattice parameters to bulk values preserved the volume (see Fig. S.7a). Band gap analysis also showed that the band gap value of 1.3 eV is obtained only for samples sulfurized at 700 °C or above (Fig. S.7b) and much lower for low temperature or unsulfurized samples.

Figure 3(b) demonstrates our findings from Raman spectroscopy. Sulfurization treatment up to 1000 °C resulted in clear increased intensity and lower FWHM. A quantitative analysis of the Raman data is shown in Table S.6. The inset of Fig. 3(b) shows the intensity ratio of the two vibrational modes with increasing sulfurization temperature. The trend in peak intensity and FWHM is clear and strong. In particular, the increase in E^1_{2g}/A_{1g} intensity ratio is most significant at temperatures above 700 °C, particularly at 850 and 1000 °C, consistent with XRD and optical measurements, thereby proving,

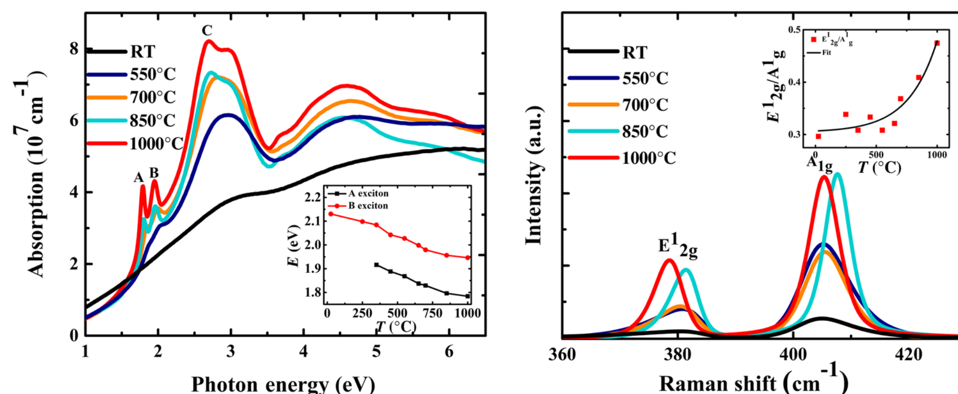

Figure 3. (a) Absorption of 12 nm-MoS_2 thin films on fused quartz. The inset demonstrates the evolution of MoS_2 A–B excitons as a function of sulfurization temperature. (b) Temperature dependent Raman spectra of 12 nm-MoS_2 thin films. The inset reveals the ratio of the Raman modes as a function of sulfurization temperature.

Downloaded from https://www.cambridge.org/core. Karolinska Institutet University Library, on 17 Aug 2018 at 17:55:22, subject to the Cambridge Core terms of use, available at https://www.cambridge.org/core/terms. https://doi.org/10.1557/mrc.2018.167

yet again, the replenishment of sulfur vacancies at higher temperatures.

While the analysis of intensity and FWHM was more straightforward, the variation in the Raman peak positions as a function of sulfurization temperature was not, particularly at 850 and 1000 °C that showed the highest XRD and Raman intensity. Most distinct were the changes in the A_{1g} peak positions at 850 °C and the E^1_{2g} peak position at 1000 °C that were different from nearby temperatures even though bulk-like frequency difference (~26 cm^{-1}) was observed at both temperatures, unlike the differences at lower sulfurization temperatures (see Table S.6). A monotonic shift in peak position was observed for E^1_{2g} peak in the 450–700 °C temperature window, while A_{1g} mode changed monotonically throughout apart from 850 °C (see Fig. S.5). The fitted linear slopes over these ranges were −0.004 and −0.0008 cm^{-1}/K for the E^1_{2g} and A_{1g} modes, respectively. In comparison, Lanzillo *et al.*[28] had much higher values (−0.015 and −0.013 cm^{-1}/K) through temperature dependent Raman measurements. The weak variation in the peak positions, therefore, showed a residual strain effect, at best, and not observed in the entire temperature range.

Figure 4(a) demonstrates the evolution of resistivity as a function of sulfurization temperature. Ohmic (linear) contacts were verified through Current–Voltage (*I*–*V*) measurements as shown in Fig. S.6a. The resistivity curve shows a non-monotonic behavior with sulfurization temperature and can be divided into four regions as shown in Fig. 4(a). In region 1 (RT-350 °C), the introduction of large sulfur atoms in vacuum-annealed, nearly metallic, MoS_2 introduces strong scattering that increases the resistivity to above the bulk value at 350 °C. The temperature in this range is not high for the sulfur atoms to reach equilibrium positions in the MoS_2 lattice. In region II (350–650 °C), the higher temperatures provide the sulfur atoms higher thermal energy to attain equilibrium crystal positions, promoting higher crystalline order, which gradually reduces the resistivity towards the bulk value. Region III (650–850 °C) provides the optimum window for growth with stable and near bulk resistivity values. Temperatures close to 1000 °C (Region IV) show a slight increase in resistivity and may indicate the presence of structural disorder due to high temperatures. Qualitatively, a similar trend was observed down to few-layer MoS_2. The optimum resistivity value of a 12 and 5 nm MoS_2 thin film is 32.07 and 83.64 Ωcm, respectively. The increase in resistivity for thinner MoS_2 could be, in part, explained as due to the change in the electronic nature in few-layer MoS_2 thin films. Hall measurements also revealed a dramatic increase in mobility and reduction of carrier concentration with sulfurization. An optimally sulfurized MoS_2 thin film (12 nm) recorded a mobility value of $\mu = 37.6 \pm 14.1$ cm^2/V/s and a carrier density $n = (7.1 \pm 2.51) \times 10^{15}$ cm^{-3}, comparable with those reported by Nazir *et al.*[29] whereas vacuum annealed samples showed very low mobility <1 cm^2/V/s and high bulk carrier concentration $n \sim 10^{21}$–10^{22} cm^{-3}.

In Fig. 4(b), we compared the photo-conductivity behavior between the optimally sulfurized (M_2 type, $T = 850$ °C) and unsulfurized (M_1 type, vacuum annealed) MoS_2. The photocurrent was measured by shinning a manually-controlled laser pulse of 5 mW power (wavelength = 532 nm) and taking the current versus voltage (*I*–*V*) data taken at intervals of 100 ms. Despite our limited resolution, the difference in the sample response was clear. A sharp, symmetric response (fall and rise time below 100 ms) is observed for the sulfurized samples compared with a slow, asymmetric photo-response for vacuum annealed samples (rise time = 1.1 s and fall time = 1.6 s). Again, this highlights the importance of sulfurization in sputtered samples. In Fig. S6(b), we showed the response of some other sulfurized samples with manually controlled pulse-width and cycle.

The conclusions from various measurements presented above share a common physical origin, i.e., sulfur vacancies are responsible for (a) weak crystal structure (b) lack of clear excitonic peaks and low band gap (c) weak Raman modes, particularly E^1_{2g}, (d) metallic transport behavior, and (e) weak photo-conducting behavior. To approximately interpret the electronic properties of sulfur deficient MoS_2 we have performed first-principles optical absorption and density of states

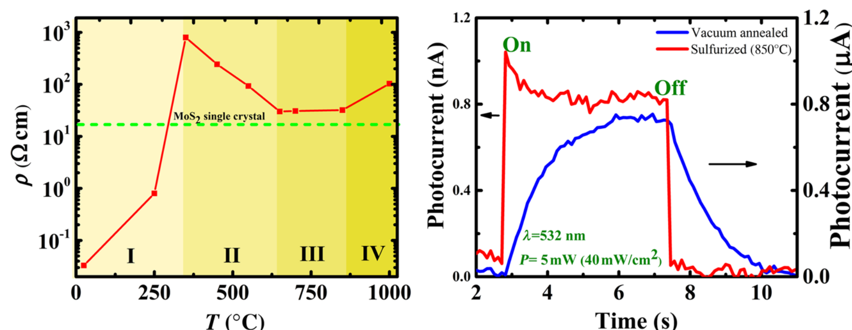

Figure 4. (a) Variation in 12 nm-MoS_2 thin film resistivity as a function of sulfurization temperature. (b) Photoconductivity measurements on a vacuum annealed (blue) and sulfurized sample (red).

Downloaded from https://www.cambridge.org/core. Karolinska Institutet University Library, on 17 Aug 2018 at 17:55:22, subject to the Cambridge Core terms of use, available at https://www.cambridge.org/core/terms. https://doi.org/10.1557/mrc.2018.167

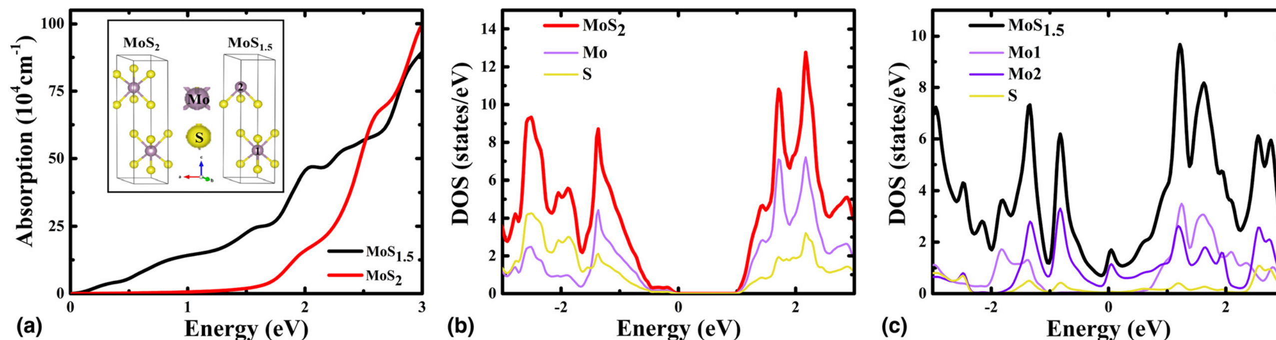

Figure 5. (a) Simulated absorption spectra of MoS_x ($x = 2$, 1.5). Inset shows the crystal structure of $MoS_{1.5}$ and MoS_2 on which the calculations were performed. (b) Density of states calculations of MoS_2. (c) Density of states calculations of $MoS_{1.5}$.

calculation of a hypothetical MoS_x ($x = 1.5$) compound and compared with stoichiometric MoS_2. Since we assume an ordered structure for $MoS_{1.5}$, the properties cannot reproduce the effect of a disordered crystal structure (weak XRD and Raman). Nonetheless, the physical insight can be highly revealing. In the inset of Fig. 5(a), we showed the unit cell of the two structures. The sulfur deficient $MoS_{1.5}$ structure was created by removing a sulfur atom from one of the two Mo atoms in the MoS_2 unit cell (denoted by atom 2 in Fig. 5(a) inset). Initially, the bulk MoS_2 structure was volume relaxed to obtain $a =$ 3.16 Å and $c/a = 3.965$ which was very close to experimental values of $a = 3.14$ Å and $c/a = 3.905$. Using this structure, we obtained an indirect band gap of nearly 1.0 eV which was lower than the experimental value (1.3 eV), but similar to other GGA calculations.[30] The Kramers-Kronig consistent optical absorption spectra of stoichiometric MoS_2 and sulfur deficient $MoS_{1.5}$ is shown in Fig. 5(a). As clear, the sulfur-deficient $MoS_{1.5}$ did not show a gapped behavior whereas stoichiometric MoS_2 showed a 1.0 eV band gap. This data is consistent with Fig. S.7 where we showed that the bulk band gap was obtained when the sulfur deficiency was completely removed (samples annealed above 650 °C), whereas vacuum annealed sample (modelled as $MoS_{1.5}$) showed a very small gap value (0.3 eV). The lack of the gapped behavior in $MoS_{1.5}$ is confirmed in the electronic density of states calculations as shown in Fig. 5(b). The stoichiometric structure showed the 1.0 eV gap, while a metallic ground state was obtained in the sulfur-deficient structure with an electronic contribution at Fermi level from the Mo atom from which the sulfur atom was removed (Mo 2). Results shown in Fig. 5(b) is consistent with experimental transport results. The resistivity and Hall measurements of RT-vacuum annealed sample (M_1) showed a nearly metallic behavior which was consistent with the computed density of states of $MoS_{1.5}$ whereas optimally sulfurized samples showed a resistivity consistent with a semiconducting behavior. Sulfur deficiency also resulted in a sluggish photo-response behavior (due to scattering from vacancy sites) which improved drastically when the vacancies are removed.

Conclusion

In conclusion, we systematically investigated the evolution of structural, optical, and transport properties in MoS_2 as a function of sulfur deficiency. We showed that an ex-situ sulfurization at high temperatures of magnetron sputtered MoS_2 (nominal composition) provided the highest quality of thin films due to the replenishment of the sulfur vacancies. Sputtered MoS_2 followed by a high-temperature sulfurization revealed a drastic enhancement of structural, interfacial, and electronic properties as demonstrated by diffraction, spectroscopic, and electronic transport techniques. High crystalline order and sharper interfaces were noted in the case of sulfurized samples. Sharp MoS_2 A–B exciton peaks were noted with increasing sulfurization temperature along with a high bulk order. Evidence of sulfur vacancies was also provided in Raman spectroscopy measurements where a strong increase in the Raman signal was noted for samples sulfurized at high temperatures. We also conclusively demonstrated that sulfur vacancies in MoS_2 thin films were responsible for the decrease in DC resistivity and slow photo-response. Our work provides atomic-level insights into the structure–property relationship of large-area TMDC films. Moreover, the proposed joint-process of PVD and CVD for the synthesis of large-area high-quality MoS_2 thin films could be extended to other 2D materials with the incorporation of slight modifications leading to a plethora of applications.

Supplementary material

The supplementary material for this article can be found at https://doi.org/10.1557/mrc.2018.167

Acknowledgments

Dipanjan Mazumdar would like to thank startup funds at Southern Illinois University (SIU) and support through the NSF-REU grant (DMR 1461255). The Raman data shown here was performed at the Frederick Seitz Materials Research Laboratory, University of Illinois at Urbana-Champaign. We

Downloaded from https://www.cambridge.org/core. Karolinska Institutet University Library, on 17 Aug 2018 at 17:55:22, subject to the Cambridge Core terms of use, available at https://www.cambridge.org/core/terms. https://doi.org/10.1557/mrc.2018.167

also thank the support provided by the SIU Advanced Coal Energy Research Center (ACERC) grant. This work used the Extreme Science and Engineering Discovery Environment (XSEDE) which is supported by National Science Foundation grant number ACI-1548562. Computational resources were provided at the San Diego Supercomputer Center (comet) through allocation DMR160135. We additionally thank Nicole Wolter of SDSC for her assistance and Milinda Wasala for assistance with AFM measurements.

References

1. S. Manzeli, D. Ovchinnikov, D. Pasquier, O. Yazyev, and A. Kis: 2D transition metal dichalcogenides. *Nat. Rev. Mater.* **2**, 17033 (2017).
2. K.S. Novoselov, A. Mishchenko, A. Carvalho, and A.H. Castro Neto: 2D materials and van der Waals heterostructures. *Science* **353**, 9439 (2016).
3. W. Zhao, Z. Ghorannevis, L. Chu, M. Toh, C. Kloc, P.H. Tan, and G. Eda: Evolution of electronic structure in atomically thin sheets of WS_2 and WSe_2. *ACS Nano* **7**, 791 (2013).
4. J.S. Ross, S. Wu, H. Yu, N.J. Ghimire, A.M. Jones, G. Aivazian, J. Yan, D. G. Mandrus, D. Xiao, W. Yao, and X. Xu: Electrical control of neutral and charged excitons in a monolayer semiconductor. *Nat. Commun.* **4**, 2498 (2013).
5. Y.H. Lee, X.Q. Zhang, W. Zhang, M.T. Chang, C.T. Lin, K.D. Chang, Y. C. Yu, J.T. Wang, C.S. Chang, L.J. Li, and T.W. Lin: Synthesis of large-area MoS_2 atomic layers with chemical vapor deposition. *Adv. Mater.* **24**, 2320 (2012).
6. A.K. Geim and K.S. Novoselov: The rise of graphene. *Nat. Mater.* **6**, 183 (2007).
7. N. Liu, P. Kim, J.H. Kim, J.H. Ye, S. Kim, and C.J. Lee: Large-area atomically thin MoS_2 nanosheets prepared using electrochemical exfoliation. *ACS Nano* **8**, 6902 (2014).
8. B. Radisavljevic and A. Kis: Mobility engineering and a metal–insulator transition in monolayer MoS_2. *Nat. Mater.* **12**, 815 (2013).
9. Z.M. Gabor, J. Peto, G. Dobrik, C. Hwang, L.P. Biro, and L. Tapaszto: Exfoliation of large-area transition metal chalcogenide single layers. *Sci. Rep.* **5**, 14714 (2015).
10. D. Dumcenco, D. Ovchinnikov, O.L. Sanchez, P. Gillet, D.T.L. Alexander, S. Lazar, A. Radenovic, and A. Kis: Large-area MoS_2 grown using H_2S as the sulphur source. *2D Mater.* **2**, 044005 (2015).
11. S. Najmaei, Z. Liu, W. Zhou, X. Zou, G. Shi, S. Lei, B.I. Yakobson, J. C. Idrobo, P.M. Ajayan, and J. Lou: Vapour phase growth and grain boundary structure of molybdenum disulphide atomic layers. *Nat. Mater.* **12**, 754 (2013).
12. Y. Yu, C. Li, Y. Liu, L. Su, Y. Zhang, and L. Cao: Controlled scalable synthesis of uniform, high-quality monolayer and few-layer MoS_2 films. *Sci. Rep.* **3**, 1866 (2013).
13. X. Li and H. Zhu: Two-dimensional MoS_2: properties, preparation, and applications. *J. Materiomics* **1**, 33 (2015).
14. K. Kang, S. Xie, L. Huang, Y. Han, P.Y. Huang, K.F. Mak, C.J. Kim, D. Muller, and J. Park: High-mobility-three-atom-thick semiconducting films with wafer-scale homogeneity. *Nature* **520**, 656 (2015).
15. L.K. Tan, B. Liu, J.H. Teng, S. Guo, H.Y. Low, and K.P. Loh: Atomic layer deposition of a MoS_2 film. *Nanoscale* **6**, 10584 (2014).
16. K.K. Liu, W. Zhang, Y.H. Lee, Y.C. Lin, M.T. Chang, C.Y. Su, C.S. Chang, H. Li, Y. Shi, H. Zhang, C.S. Lai, and L.J. Li: Growth of large-area and highly crystalline MoS_2 thin layers on insulating substrates. *Nano Lett.* **12**, 1538 (2012).
17. M.I. Serna, S.H. Yoo, S. Moreno, Y. Xi, J.P. Oviedo, H. Choi, H.N. Alshareef, M.J. Kim, M. Minary-Jolandan, and M.A. Quevedo-Lopez: Large-area deposition of MoS_2 by pulsed laser deposition with in situ thickness control. *ACS Nano* **10**, 6054 (2016).
18. D. Fu, X. Zhao, Y.Y. Zhang, L. Li, H. Xu, A.R. Jang, S.I. Yoon, P. Song, S. M. Poh, T. Ren, Z. Ding, W. Fu, T.J. Shin, H.S. Shin, S.T. Pantelides, W. Zhou, and K.P. Loh: Molecular beam epitaxy of highly crystalline monolayer molybdenum disulfide on hexagonal boron nitride. *J. Am. Chem. Soc.* **139**, 9392 (2017).
19. J. Tao, J. Chai, X. Lu, L.M. Wong, T.I. Wong, J. Pan, Q. Xiong, D. Chi, and S. Wang: Growth of waferscale MoS_2 monolayer by magnetron sputtering. *Nanoscale* **7**, 2497 (2015).
20. H. Samassekou, A. Alkabsh, M. Wasala, M. Eaton, A. Walber, A. Walker, O. Pitkänen, K. Kordas, S. Talapatra, T. Jayasekera, and D. Mazumdar: Viable route towards large-area two dimensional MoS_2 using magnetron sputtering. *2D Mater.* **4**, 021002 (2017).
21. M. Wasala, J. Zhang, S. Ghosh, B. Muchharla, R. Malecek, D. Mazumdar, H. Samassekou, M. Gather-Ganim, A. Morrison, N.P. Lopez, V. Carozo, Z. Lin, M. Terrones, and S. Talapatra: Effect of underlying boron nitride thickness on photocurrent response in molybdenum disulfide - boron nitride heterostructures. *J. Mater. Res.* **31**, 893 (2016).
22. J. Towns, T. Cockerill, M. Dahan, I. Foster, K. Gaither, A. Grimshaw, V. Hazlewood, S. Lathrop, D. Lifka, G.D. Peterson, R. Roskies, R. J. Scott, and N. Wilkins-Diehr: XSEDE: accelerating scientific discovery. *Comput. Mater. Sci.* **16**, 62 (2014).
23. P. Blaha, K. Schwarz, G.H. Madsen, D. Kvasnicka, and D. Luitz: *WIEN2k, an Augmented Plane Wave + Local Orbitals Program for Calculating Crystal Properties* (Vienna: Technische Universität Wien, 2001).
24. J. P. Pedrew, S. Burke, and M. Ernzehof: Generalized gradient approximation made simple. *Phys. Rev. Lett.* **77**, 3865 (1996).
25. S. Grimme, J. Antony, S. Ehrlich, and H. Krieg: A consistent and accurate ab initio parametrization of density functional dispersion correction (DFT-D) for the 94 elements H-Pu. *J. Chem. Phys.* **132**, 154104 (2010).
26. K.F. Mak, C. Lee, J. Hone, J. Shan, and T.F. Heinz: Atomically thin MoS_2: a new direct-gap semiconductor. *Phys. Rev. Lett.* **105**, 136805 (2010).
27. J.E. Padilha, H. Peelaers, A. Janotti, and C.G. Van de Walle: Nature and evolution of the band-edge states in MoS_2: From monolayer to bulk. *Phys. Rev. B* **90**, 205420 (2014).
28. N. Lanzillo, A. Birdwell, M. Amani, F. Crowne, P. Shah, S. Najmaei, Z. Liu, P. Ajayan, J. Lou, M. Dubey, S. Nayak, and T. O'Regan: Temperature-dependent phonon shifts in monolayer MoS_2. *Appl. Phys. Lett.* **103**, 093102 (2013).
29. G. Nazir, M. F. Khan, V. M. Lermolenko, and J. Eom: Two- and four-probe field-effect and Hall mobilities in transition metal dichalcogenide fieldeffect transistors. *RSC Adv.* **6**, 60787 (2016).
30. S. Bhattacharyya and A. K. Singh: Semiconductor-metal transition in semiconducting bilayer sheets of transition-metal dichalcogenides. *Phys. Rev. B* **86**, 075454 (2012).

Downloaded from https://www.cambridge.org/core. Karolinska Institutet University Library, on 17 Aug 2018 at 17:55:22, subject to the Cambridge Core terms of use, available at https://www.cambridge.org/core/terms. https://doi.org/10.1557/mrc.2018.167